Local Path Planning for Autonomous Vehicles: Crash Mitigation

Hong Wang, Yanjun Huang*, Amir Khajepour, Teng Liu, Yechen Qin, Yubiao Zhang

Abstract— **A path planning approach to generate a path which mitigates the effects of an inevitable crash for autonomous vehicles is presented in this brief. The model predictive control algorithm is adopted here for path planning. The artificial potential field, which describes the obstacles and the potential crash severity, are added to the control objectives to avoid the obstacle, and also to mitigate the inevitable crash. The vehicle dynamic is also considered as an optimal control objective. Based on the analysis above, the model predictive controller can guarantee the command following, obstacle avoidance, vehicle dynamics, and mitigate the inevitable crash. Simulation results verified that the proposed MPC has the abilities of obstacles avoidance and mitigation of the inevitable crash.**

Index Terms—Crash Mitigation, Potential Crash Severity, Autonomous Vehicles, Path Planning, MPC, Safety

I. INTRODUCTION

Traffic accidents are the most dangerous killer in the world. Statistics show that there are millions of humans who have lost their lives under the wheel of vehicles. Some advanced driving assistance systems (ADAS), for instance, cruise control, adaptive cruise control (ACC) and the cooperative ACC applied in highway driving and automatic parking, blind angle vehicle detection applied in the urban environment, have improved safety significantly [1]. Fully autonomous vehicles (AVs) on the road, without human interventions, can significantly reduce accidents due to driver's errors, fatigue, and drunk driving. Full avoidance of traffic accidents is still unrealistic and determining how to generate a path with the lowest crash severity in the event of unavoidable accident situations is a challenge that needs to be studied and addressed.

According to a vehicle accidents survey [2], most accident scenes can be classified as follows: the frontal vehicle suddenly makes a turn or changes its lane without displaying a turn signal; the front vehicle suddenly brakes; an obstacle falls down from a vehicle in front; collision with a pedestrian and collision with a static car on the road. The damage caused by the accident depends on the nature of the obstacle (pedestrian, car, or road boundary, etc.), the crash speed, and its configuration [3]. For the car-car collision, the crash mainly depends on the crash speed, the direction of collision [4], the vehicle mismatch [5], the characteristics of driver such as gender, age, and weight [6], size of cars [7], and vehicle safety devices [8].

Path planning research has been a popular subject for the last few decades [15]. Many techniques have been adopted for path planning. These path planning approaches can be classified into three species: graph search-based planners, sampling-based method and interpolating curve planners. In the scope of graph search based planners, the Dijkstra algorithm is a graph search based algorithm can find the single-source shortest path in the graph [16]; A* algorithm is a graph search based algorithm enables a fast node search due to the implementation of heuristics [17]; and the state lattice algorithm uses a discrete representation of the planning area with a grid of states [18]. The Probabilistic Roadmap Method (PRM) [19] and the Rapidly-Exploring Random Tree (RRT) [20] are the most common methods of sampling-based planners. The interpolating curve planners implement different techniques for path smoothing and curve generation, such as lines and circles [21], clothoid curves and polynomial curves.

Path optimization based techniques have become the state-of-the-art AV path planning approaches in recent years [9]. The core of this technique is formulating the path planning problem as an optimization problem taking into account the multi-constraints and expected vehicle performance. Model Predictive control (MPC) has proven to be well suited for solving the path planning problem, because of their ability to handle multi-constraints and convex problems [10][22]. Besides, MPC solves the path optimization problems in a recursive manner while taking into account the updates of the environment states during its planning process. Consequently, MPC is utilized to solve the path planning problem in this brief.

To our best knowledge, crash mitigation research is still a blank area in path planning area research. We synthesize an MPC path planning controller for an autonomous vehicle which can avoid obstacles and generate an emergency path with the lowest inevitable crash severity. In the model predictive controller, predicted crash severity, the artificial potential field of obstacles and road boundaries, path following matrix and other vehicle performance constraints are taken into account of the cost function. Different scenarios are simulated to verify that our proposed control strategy has the ability to generate the path that can both avoid obstacles and mitigate the crash severity to maintain the best safety of the automated vehicles.

This paper works on the path planning algorithm for automated vehicles to mitigate crash severity once collision couldn't be avoided. Section II presents the control design for the crash mitigation path planning – including modeling of the vehicle, the definition of crash severity factor, potential field adopted here represent environment and control design for path planning. Section III presents two case studies to verify the proposed control strategy for crash

Hong Wang, Yanjun Huang, Amir Khajepour, Teng Liu and Yubiao Zhang are with the Mechanical and Mechatronics Engineering Department, University of Waterloo, Waterloo, ON. N2L 3G1, Canada.

Yechen Qin is with Department of Mechanical and vehicle engineering, Beijing Institute of Technology.

mitigation path planning and is followed by the conclusion and future work in Section IV.

II. PATH PLANNING

This section introduces the control design for crash mitigation based path planning approach for automated vehicles. The process includes modeling of the vehicle, the definition of severity factor SF, the introduction of the artificial potential field and the MPC algorithm for path planning.

A. Modeling of the vehicle

The vehicle dynamics, in reality, are very complicated, and high fidelity models may be highly non-linear and discontinuous. To design the controller, a bicycle model is used. Fig. 1 depicts a diagram of the vehicle model which has 3 degrees of freedom, i.e. longitudinal, lateral and yaws [11]:

Figure 1. Vehicle bicycle model
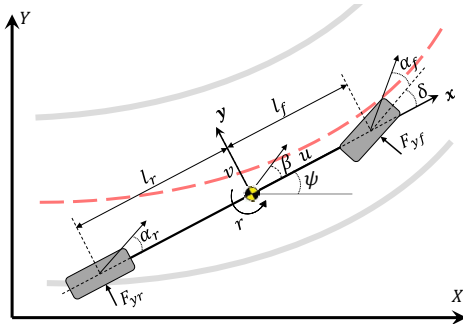
$$m(\dot{u} - vr) = F_{xT} \tag{1}$$

$$m(\dot{v} + ur) = F_{yf} + F_{yr} \tag{2}$$

$$I_z \dot{r} = F_{yf} l_f - F_{yr} l_r \tag{3}$$

The vehicle's motion with respect to global coordinates:

$$\dot{X} = u\cos\psi - v\sin\psi \quad , \quad \dot{Y} = u\sin\psi + v\cos\psi \tag{4}$$

where, m denotes total mass of the vehicle, and I_z is the vehicle 's yaw moment of inertia; r, u, and v are yaw rate at CG, velocity in longitudinal direction, and lateral velocity, respectively. l_r, l_f are the distance from C.G. to the front and rear axle. X and Y are the vehicle position in longitudinal and lateral directions, ψ is the heading angle of the vehicle, F_{yr} and F_{yf} denotes the rear and front tire forces, F_{xT} is the longitudinal tire forces.

The tire forces in lateral direction of the front-wheel steering vehicle with a linear tire model can be calculated as:

$$F_{yf} = -C_{\alpha f}\alpha_f = C_{\alpha f}\left(\delta - \frac{v + l_f r}{u}\right) \tag{5}$$

$$F_{yr} = -C_{\alpha r}\alpha_r = C_{\alpha r}\left(-\frac{v - l_r r}{u}\right) \tag{6}$$

where δ is the input steering angle, α_f denotes the sideslip angle of front tire, α_r denotes the rear tires' sideslip angles, $C_{\alpha f}$ and $C_{\alpha r}$ represent the front and rear tires' cornering stiffness.

B. Definition of Potential Crash Severity Index PCSI

As presented in the introduction, the accident severity mainly depends on the crash speed, the obstacle characteristics, and the hitting configuration (front collision with a stopped vehicle, with a rigid fixed obstacle, or with any other vehicles). Three main factors are considered in this paper: the speed of crash, the crash angle, and the mass ratio of two collision vehicles.

1) Relative Speed ΔV

Many speed related metrics are adopted to evaluate the potential crashes severity, which includes the equivalent speed, the energy equivalent speed, the acceleration severity index, or occupant impact velocity. From the collision data analysis for the U.S., Britain, and Australia, the crash severity relating to the speed is a function of ΔV, which is the vehicle speed change before and after the crash moment. Instead, but essentially the same, the approaching velocity is adopted as the definition of the ΔV to measure potential crash severity index (PCSI) in our algorithm:

$$PCSI(\Delta V) = \frac{\Delta V}{D} \tag{7}$$

where, ΔV and D are the approaching velocity and the distance between the obstacle vehicle and the ego vehicle, respectively.

2) Relative heading Angle θ

Databased analysis showed that the highest crash risk occurred in 1/3 overlap crashes while equivalent barrier speed higher than 20 mph [13]. Based on the above analysis and for the convenience of implementation, we define the relative angle θ between the ego vehicle and obstacle vehicle as the sum of the heading angle of each vehicle. The potential crash severity index related to the relative angle θ is defined as below:

$$PCSI(\theta) = \begin{cases} 1 & \theta = 0^0 \ \& \ 180^0 \\ 4 & \theta = 0^0 \sim 15^0 \ \& \ 165^0 \sim 180^0 \\ 3 & \theta = 15^0 \sim 45^0 \ \& \ 135^0 \sim 165^0 \\ 2 & \theta = 45^0 \sim 90^0 \ \& \ 90^0 \sim 135^0 \end{cases} \tag{8}$$

3) Mass Ratio W_o/W

In terms of mismatch in two-vehicle crashed, reports showed that the death relative risk for occupants in light truck vehicle is 3 to 4 times greater than those involved in crashes with passenger vehicle [7]. Regarding the potential crash severity index related to the mass ratio of the two vehicles, we can simply define it as below [14]:

$$PCSI(W) = \frac{W_o}{W} \tag{9}$$

1603

where W_o and W are the weight of the obstacle vehicle and the ego vehicle, respectively. As a result, the total potential crash severity index will be:

$$PCSI = f(\Delta V, \theta, W_O / W) = k_{\Delta v} PCSI(\Delta V) + k_\theta PCSI(\theta) + k_w PCSI(W) \tag{10}$$

where, $k_{\Delta v}$, k_θ, and k_w are the weight parameters of potential crash severity related to the relative speed, relative angle and mass ratio, respectively.

C. Obstacle description

There are three kinds of obstacles defined by the artificial potential field (PF), non-crossable (U_{NC}), crossable (U_C) and the road (U_R). The potential field can be calculated as the sum of the PFs [23]:

$$U = \sum_i U_{NC_i} + \sum_j U_{C_j} + \sum_q U_{R_q} \tag{11}$$

where indices i, j, and q represent the i_{th} obstacle that cannot be crossed, the j_{th} obstacle that can be crossed, and the q_{th} lane marker, respectively. The detailed introduction of these three PFs is described below:

a) Non-crossable Obstacle:

Non-crossable obstacles such as a vehicle or a pedestrian can cause instability, damage to vehicle or threaten peoples' lives and is as a function of safe distance SD, s_i [12]:

$$U_{NC_i}(X,Y) = \frac{a_i}{s_i^{b_i}} = \frac{a_i}{s_i(\frac{dX}{X_{si}}, \frac{dY}{Y_{si}})^{b_i}}$$

$$X_{si} = X_0 + uT_0 + \frac{\Delta u_{a_i}^2}{2a_n} \tag{12}$$

$$Y_{si} = Y_0 + (u \sin\theta_e + u_{oi} \sin\theta_e)T_0 + \frac{\Delta v_{a_i}^2}{2a_n}$$

where a_i and b_i are the shape and intensity parameters of the PF, respectively, X_{si} denotes the longitudinal safe distacne from the obstacle, Y_{si} is the lateral safe distances from the obstacle, X_o and Y_o are the minimum longitudinal and lateral distance. To denote the safe time gap, u represents the ego vehicle's velocity, and u_{oi} is obstacles' velocity, θ_e is the heading angle towards each other. The potential field for the non-crossable obstacle located at (20m, 2m) is presented in Fig.2.

Figure 2. PF of non-crossable obstacle
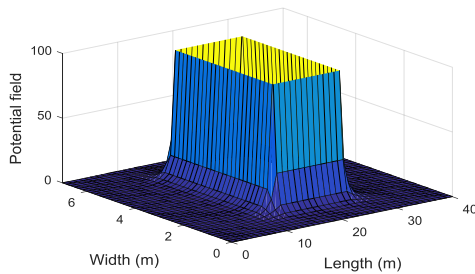
b) Crossable Obstacle:

An exponential function is used to define the PF of some obstacles such as a little bump or some soft garbage on the road cannot cause any damage to the ego vehicle:

$$U_{C_j}(X,Y) = a_j e^{-b_j s_j} = a_j e^{-b_j s_j(\frac{dX}{X_{si}}, \frac{dY}{Y_{si}})} \tag{13}$$

where a_j and b_j are the shape and intensity parameters of the obstacle, s_j represents the normalized safe distance between the obstacle and the ego vehicle calculated similarly to (12). The potential field for the crossable obstacle located at (10m, 2m) is depicted in Fig.3.

Figure 3. PF of crossable obstacle
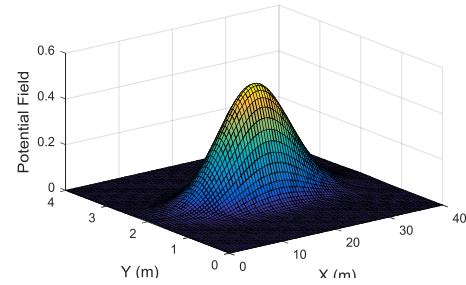
c) Road boundary:

When the ego vehicle drives on the road, especially on the highway, the vehicle cannot cross the road lane marker unless the driver intends to change lanes. Hitting the road isolated belt is forbidden, as it can cause instability or serious car crash. To avoid road crossings that are undesired, PFs for road boundary can be defined as:

$$U_{R_q}(X,Y) = \begin{cases} a_q(S_{Rq}(X,Y) - D_a)^2 & S_{Rq}(X,Y) < D_a \\ 0 & S_{Rq}(X,Y) > D_a \end{cases} \tag{14}$$

where s_{Rq} is the vehicle safe distance from the road boundary, D_a is the permitted distance from the road boundary, q denotes the lane marker of the right or left side, and a_q is the intensity parameters.

Quadratic functions are utilized to define the lane marker PFs, and when the safe distance decreases, their gradients linearly increase, as shown in Fig.4.

Figure 4. PF of road boundary
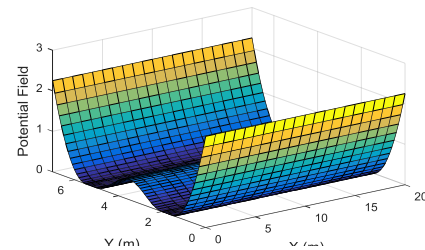
D. Control Design for Path Planning

The model predictive control algorithm is adopted here for path planning in this Section. The presented crash severity factor and artificial potential field are calculated to the objective function to achieve the goal of obstacle avoidance and the lowest crash severity. The vehicle dynamic is also considered as an optimal control problem. Based on the analysis above, the model predictive controller can optimize the command following, obstacle avoidance, vehicle dynamics, road regulation and mitigate the inevitable crash with the predicted values.

It is presumed that the path planning module accepts the information of the desired lane, speed, the obstacles, the road boundaries, and the vehicles states.

Using equations (1)-(6), the vehicle's dynamics in global coordinates can be written in state space form as:

$$\dot{x} = Ax + Bu \qquad (15)$$

$$y = Cx \qquad (16)$$

where, $x = [X \ u \ Y \ v \ \psi \ r]^T$, $u = [F_{xT} \ \delta]^T$, $y = [Y \ u]^T$. State matrix includes longitudinal and lateral position X, Y; the lateral and longitudinal velocity, v, u; heading angle ψ and yaw rate of the vehicle r. System inputs consist of the longitudinal tire force F_{xT} and steering angle δ. y is the output matrix including lateral position and velocity.

The desired output matrix including the desired lane and the target longitudinal velocity represents the reference to be tracked is shown as below:

$$\mathbf{y_{des}} = [Y_{des} \ u_{des}]^T \qquad (17)$$
$$Y_{des} = (l_{des} - 1/2)L_w$$

where y_{des} is the desired output matrix including the desired vehicle lateral position Y_{des} and desired velocity u_{des}. l_{des} is the desired lane index number counted from the right-hand side. L_w is the width of the lane.

One of the advantages of MPC is its capability to deal with constraints on not only the input but also the state and output. Therefore, the constraints including the road regulations, actuator capacity constraints, and the vehicle dynamic constraints are considered into this MPC problem.

First of all, the road vehicle should not violate the requirements of the maximum and minimum speed according to the road regulations. The constraints can be expressed as:

$$u_{min} < u < u_{max} \qquad (18)$$

where u_{min} and u_{max} denote the minimum and maximum allowed speed.

In addition, the actuator capacities are considered as:

$$|\delta| \le \delta_{max,}$$
$$F_x \le \frac{T_{max}}{R_{eff}}, \qquad (19)$$
$$|\Delta \delta| \le \Delta \delta_{max}$$

where R_{eff} denotes the wheels' radius; δ_{max} denotes the maximum steering angle; T_{max} is the maximum propelling torque; $\Delta \delta$ is the rate of change of steering angle in one step, and $\Delta \delta_{max}$ is its capacity.

The longitudinal load transfer efficiency is included in the tire force ellipse constraints:

$$\left(\frac{F_{xT}}{F_{xT\_max}}\right)^2 + \left(\frac{F_{yf}}{F_{yf0\_max}} \cdot \frac{Wl_r}{Wl_r - F_{xT}h}\right)^2 \le \mu^2$$
$$\left(\frac{F_{xT}}{F_{xT\_max}}\right)^2 + \left(\frac{F_{yr}}{F_{yr0\_max}} \cdot \frac{Wl_f}{Wl_f + F_{xT}h}\right)^2 \le \mu^2 \qquad (20)$$

where F_{xT_max} represents the maximum total longitudinal tire force. F_{yf0_max} and F_{yr0_max} denote the nominal maximum lateral front and rear tire force. W is the weight of the vehicle. h is the height of the C.G.. μ is the tire-road friction coefficient.

The cost function including the potential field U, severity factor SF, the tracking of the desired path, control input as well as its variation, and slack variables is shown as:

$$\min_{u_c,\varepsilon} J = \min_{u_c,\varepsilon} \sum_{k=1}^{N_p} \mathbf{U}^{t+k,t} + PCSI^{t+k,t} + \left\| \mathbf{y}^{t+k,t} - \mathbf{y}_{des}^{t+k,t} \right\|_Q^2 + \left\| \mathbf{u}_c^{t+k-1,t} \right\|_R^2$$
$$+ \left\| \mathbf{u}_c^{t+k-1,t} - \mathbf{u}_c^{t+k-2,t} \right\|_S^2 + \left\| \varepsilon_k \right\|_P^2 \qquad (21)$$

$$s.t.(k = 1,...N_p)$$

$$x^{t+k,t} = \mathbf{A}_d x^{t+k-1,t} + \mathbf{B}_d \mathbf{u}_c^{t+k-1,t} \qquad (21.a)$$

$$y^{t+k,t} = \mathbf{C}x^{t+k,t} + \mathbf{D}\mathbf{u}_c^{t+k,t} \qquad (21.b)$$

$$y_s^{t+k,t} = \mathbf{C}_s x^{t+k,t} + \mathbf{D}_s \mathbf{u}_c^{t+k,t} \qquad (21.c)$$

$$y_s^{t+k,t} \le y_{s\_max}^{t+k,t} + \varepsilon \qquad (21.d)$$

$$\varepsilon_k \ge 0 \qquad (21.e)$$

$$\mathbf{u}_{c\_min} < \mathbf{u}_c^{t+k-1,t} < \mathbf{u}_{c\_max} \qquad (21.f)$$

$$\Delta \mathbf{u}_{c\_min} < \mathbf{u}_c^{t+k-1,t} - \mathbf{u}_c^{t+k-1,t} < \Delta \mathbf{u}_{c\_max} \qquad (21.g)$$

$$u_c^{t+k,t} = u_c^{t+k-1,t}, k \ge N_c, k \ne c_2 N_{rc} + N_c, c_2 = 1,...(N_p - N_c)/N_{rc} \qquad (21.h)$$

$$u_c^{t-1,t} = u_c(t-1) \qquad (21.i)$$

$$x^{t,t} = x(t) \qquad (21.j)$$

where $t+k$ represents the k steps' predicted value ahead of the current time t. N_c and N_p denote the control horizon and the prediction horizon, respectively. ε_k is the slack variables vector for k steps, representing the penalty of soft constraints of tire forces. The objective function contains the potential field, the crash severity, the path tracking, inputs, inputs changes, and slack variables. Among them, the path tracking, inputs, inputs changes, and slack variables are added with weighting matrices Q, R, S, and the first norm of slack variables weighted with P, respectively. The states are predicted through (21.a). Equation (21.b) generates the outputs, where C is the output and D is the feedforward matrix. The constraints on the actuators, the vehicle speed and corresponding linear constraints of the tire capacity constraints are presented in (21.d), where y_s is the soft constraint variables vector and is also included to provide permission of the bounds violation. The slack variables corresponding to actuator constraints are set to zero since they cannot be violated. The linearized constraints that can be written as a function of the inputs and states in (21.c), where D_s and C_s denote the feedforward and the output matrices, respectively. The vehicle speed and its violation limitation are represented in (21.f) and (21.g). The computation cost can be reduced by decreasing the control

1605

inputs number in (21.h), and the control inputs change every N_{rc} steps after the first N_c prediction steps.

III. CASE STUDY

The parameters of the autonomous vehicle and the controller are illustrated in Table I.

TABLE I
PARAMETERS OF AUTONOMOUS VEHICLE AND THE CONTROLLER

Parameter	Value	Unit	Parameter	Value	Unit
m	2270	kg	a_{max}	9	m/s^2
h	0.647	m	a_n	1	m/s^2
l_f	1.421	m	D_a	0.5	m
l_r	1.434	m	N_p	20	--
I_z	4600	Kgm^2	N_c	5	--
C_f	127000	N	N_{rc}	5	--
C_r	130000	N	Q	[0.2 0.01]	
μ	0.9	--	R	[2e-9 100]	
R_{eff}	0.351	m	X	[5e-8 500]	
F_{xt_max}	21400	N	δ_{max}	10	deg
F_{yf0_max}	10400	N	$\Delta \delta_{max}$	0.5	deg
F_{yr0_max}	10600	N	T_{max}	3000	Nm

Case study 1: As shown in Fig. 5, the ego vehicle starts on lane 1 with the speed of 60km/h, meanwhile there is an obstacle vehicle in the middle of lane 2, 10m ahead. The pedestrian crossing area on lane 1 is full. However, there is no isolation belt for the road boundary. In this situation, the crash is inevitable as there is not enough space between vehicle 1 and pedestrian for stopping the vehicle, and lane 2 is not clear.

Figure 5.   Schematic diagram of case study 1
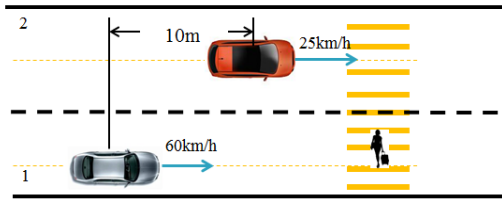
Using the method described in the work, the lateral distance of the ego vehicle is shown in Fig.6. As can be seen, the vehicle chooses to cross the road boundary rather than to hit pedestrians and the left-hand vehicle. The velocity is shown in Fig.7 which can be seen that the ego vehicle also takes harsh brake to cross the road boundary. Fig.8. demonstrates the front tire force of the ego vehicle.

Figure 6.   Lateral distance of ego vehicle
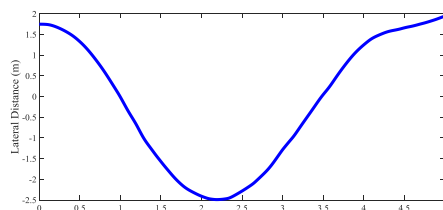

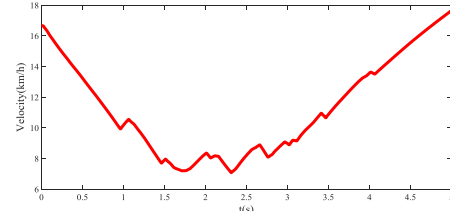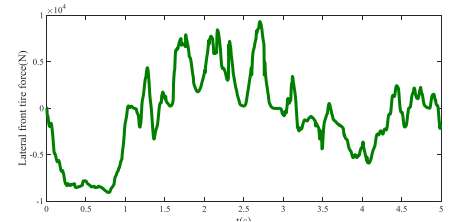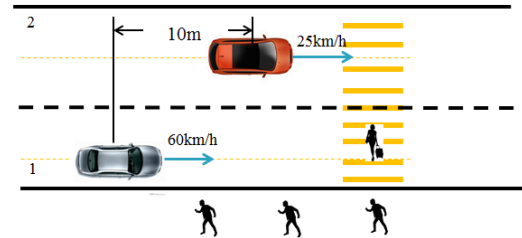Figure 7.   Longitudinal velocity of the ego vehicle

Figure 8.   Lateral front tire force of the ego vehicle

Case study 2: The ego vehicle starts on Lane 1 with the speed of 60km/h. There is an obstacle vehicle 1 in the middle of Lane 2 with the speed of 25km/h and is initially 10m ahead of the obstacle in X-direction. The pedestrian crossing section and also the right sidewalk are both occupied by pedestrians. Meanwhile, the left sidewalk is empty. The situation is designed such that the ego vehicle cannot avoid both obstacles while it stays within the road boundaries. The schematic diagram is depicted in Fig. 9.

Figure 9.   Schematic diagram of case study 2

The trajectory of the ego vehicle is shown in Fig.10. In this situation, the ego vehicle avoids hitting pedestrians and minimizes the accident severity by entering to the left lane. Fig.11 shows the longitudinal velocity of the ego vehicle. Fig.12 demonstrates the front tire force of the ego vehicle. To our best knowledge, the human life's protection is a summum bonum. The simulation results meet the requirements of the moral rules for connected and automated vehicular traffic.

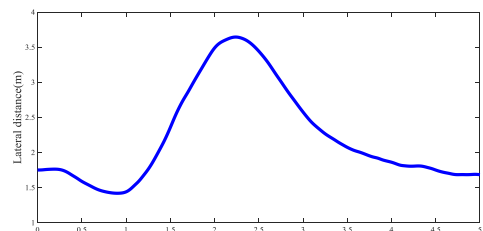Figure 10.   Lateral distance of ego vehicle

1606

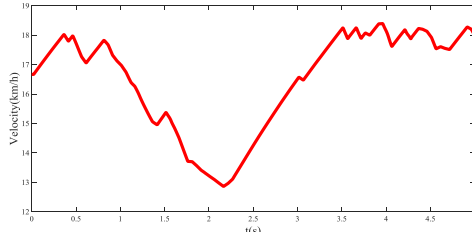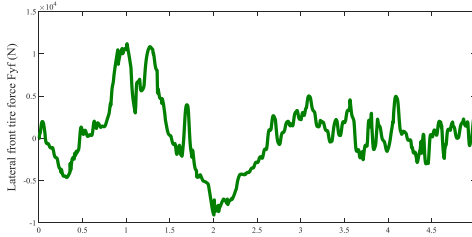Figure 11.   Longitudinal velocity of the ego vehicle

Figure 12.   Lateral front tire force of the ego vehicle

IV. CONCLUSION

A path planning method was proposed for autonomous vehicles especially when the collision is inevitable, by generating a trajectory to mitigate crash as much as possible. It is presumed that the motion planning module receives desired lane and speed information from global planning module, and the information of obstacles and the road boundaries from the perception module. In this study, the model predictive control algorithm was adopted for path planning. The presented crash severity factor and artificial potential field to describe the obstacles were inserted to the cost function to achieve the goals of obstacle avoidance and the lowest crash severity if avoidance is impossible. Furthermore, the vehicle dynamic was also considered into this optimal control problem to ensure the feasibility of the generated path.

Simulation results demonstrated that the MPC algorithm was able to avoid obstacles and mitigate the crash if a collision was inevitable. Field testing of this proposed path planning method is on the way and more urban situations should be analyzed in the future, such as emergency situations at the traffic lights.

REFERENCES

[1]   Chuan Hu, Hui Jing, Rongrong Wang, Mohammed Chadli, and Fengjun Yan, "Robust H∞ Output-Feedback Control for Path Following of Autonomous Ground Vehicles," Mechanical Systems and Signal Processing, vol. 70-71, pp. 414-427, Mar. 2016.

[2]   Chuan Hu, Rongrong Wang, and Yechen Qin, "Adaptive Multivariable Super-Twisting Control for Lane Keeping of Autonomous Vehicles with Differential Steering," 2018 IEEE Intelligent Vehicles Symposium (IV).

[3]   China.Gallen, Romain, et al. "Supporting drivers in keeping safe speed in adverse weather conditions by mitigating the risk level." IEEE Transactions on Intelligent Transportation Systems 14.4 (2013): 1558-1571.

[4]   D. Buzeman, D. Viano, and P. Lovsund, "Injury probability and risk in frontal crashes: Effects of sorting techniques on priorities for offset testing," Accid. Anal. Prev., vol. 30, no. 5, pp. 583–595, Sep. 1998.

[5]   E. Miltner and H. Salwender, "Influencing factors on the injury severity of restrained front seat occupants in car-to-car head-on collisions," Accid. Anal. Prev., vol. 27, no. 2, pp. 143–150, Apr. 1995.

[6]   E. Romano, T. Kelley-Baker, and R. Voas, "Female involvement in fatal crashes: Increasingly riskier or increasingly exposed?" Accid. Anal. Prev., vol. 40, no. 5, pp. 1781–1788, Sep. 2008.

[7]   S. Acierno, R. Kaufmanc, F. Rivara, and D. Grossman, "Vehicle mismatch: Injury patterns and severity," Accid. Anal. Prev., vol. 36, no. 5, pp. 761–772, Sep. 2004.

[8]   D. Gabauer and H. Gabler, "Comparison of roadside crash injury metrics using event data recorders," *Accid. Anal. Prev.*, vol. 40, no. 2, pp. 548– 558, Mar. 2008.

[9]   P. Liu and U̇. O̍ zgu̍ ner, "Predictive control of a vehicle convoy considering lane change behavior of the preceding vehicle," in 2015 *American Control Conference (ACC). IEEE*, 2015, pp. 4374–4379.

[10] Wang, Hong, et al. "A Novel Energy Management for Hybrid Off-road Vehicles without Future Driving cycles as A Priori." Energy (2017).

[11] Zhang, Yubiao, et al. "A comparative study of equivalent modelling for multi-axle vehicle." *Vehicle System Dynamics* (2017): 1-18.

[12] Chuan Hu, Rongrong Wang, Fengjun Yan, Yanjun Huang, Hong Wang and Chongfeng Wei, "Differential Steering Based Yaw Stabilization Using ISMC for Independently Actuated Electric Vehicles,*" IEEE Transactions on Intelligent Transportation Systems*, vol. 19, 2018.

[13] Ragland, C., and G. Dalrymple. "Overlap car-to-car tests compared to car-to-half barrier and car-to-full barrier tests." *AUTO & TRAFFIC SAFETY* 1.2 (1994).

[14] Lund, Adrian K., et al. Crash compatibility issue in perspective. No. 2000-01-1378. *SAE Technical Paper*, 2000.

[15] M. Elbanhawi and M. Simic, "Sampling-based robot motion planning: A review," *IEEE Access*, vol. 2, pp. 56–77, 2014.

[16] F. Marchese, "Multiple mobile robots path-planning with mca," in *Proc. ICAS*, Jul. 2006, p. 56.

[17] M. Likhachev and D. Ferguson, "Planning long dynamically feasible maneuvers for autonomous vehicles," Int. J. Robot. Res., vol. 28, no. 8, pp. 933–945, Aug. 2009.

[18] M. Pivtoraiko and A. Kelly, "Efficient constrained path planning via search in state lattices," in Proc. Int. Symp. Artif. Intell., Robot., Autom.Space, 2005, pp. 1–7.

[19] L. E. Kavraki, P. Svestka, J.-C. Latombe, and M. H. Overmars, "Probabilistic roadmaps for path planning in high-dimensional configuration spaces," *IEEE Trans. Robot. Autom.*, vol. 12, no. 4, pp. 566–580, Aug. 1996.

[20] S. M. LaValle and J. J. Kuffner, "Randomized kinodynamic planning," *Int. J. Robot. Res.*, vol. 20, no. 5, pp. 378–400, 2001.

[21] Xiaolin Tang*, Wei Yang, Xiaosong Hu, Dejiu Zhang. A novel simplified model for torsional vibration analysis of a series-parallel hybrid electric vehicle. *Mechanical Systems and Signal Processing.*

[22] D.Walton and D. Meek, "A controlled clothoid spline," *Comput. Graph.*, vol. 29, no. 3, pp. 353–363, Jun. 2005.

[23] Huang, Yanjun, et al. "Model predictive control power management strategies for HEVs: A review." *Journal of Power Sources* 341 (2017): 91-106.